Title

Suspension state promotes metastasis of breast cancer cells by up-regulating cyclooxygenase-2

Journal

Theranostics, 8(14)

ISSN

1838-7640

Authors

Zhang, Xiaomei
Yang, Li
Chien, Shu
et al.

Publication Date

2018

DOI

10.7150/thno.25434

Peer reviewed

IVYSPRING INTERNATIONAL PUBLISHER

Theranostics

2018; 8(14): 3722-3736. doi: 10.7150/thno.25434

Research Paper

Suspension state promotes metastasis of breast cancer cells by up-regulating cyclooxygenase-2

Xiaomei Zhang[1,2], Li Yang[1,2], Shu Chien[3], and Yonggang Lv[1,2] ✉

1. Key Laboratory of Biorheological Science and Technology (Chongqing University), Ministry of Education, Bioengineering College, Chongqing University, Chongqing 400044, P. R. China
2. Mechanobiology and Regenerative Medicine Laboratory, Bioengineering College, Chongqing University, Chongqing 400044, P. R. China
3. Departments of Bioengineering, Institute of Engineering in Medicine, University of California, San Diego, La Jolla, CA 92093, USA

✉ Corresponding author: Dr. Yonggang Lv, Professor; Mechanobiology and Regenerative Medicine Laboratory, Bioengineering College, Chongqing University, 174 Shazheng Street, Shapingba District, Chongqing 400044, China; Tel: 86-23-65102507; Fax: 86-23-65102507; E-mail: yglv@cqu.edu.cn

Received: 2018.02.08; Accepted: 2018.04.25; Published: 2018.06.12

Abstract

Hematogenous metastasis requires tumor cells to detach from primary tumor into blood/lymphatic circulation and extravasate. Tumor cells in the blood circulation system, named circulating tumor cells (CTCs), are in a suspension state, with unique cytoskeletal structure and molecular phenotype different from primary tumor cells. The aim of this study is to assess the impact of suspension state on the metastatic potential of breast cancer cells (BCCs) and study its underlying mechanism.

Methods: BCCs were cultured on low-adhesion plates to mimic the suspension state. Conventional adherent culture BCCs were used as the control. This study examined the metastatic potential of adherent and suspension BCCs *in vitro* and *in vivo*. RNA sequencing analysis, siRNA, and inhibitors were used to determine the underlying molecular mechanism.

Results: The suspension state significantly increased the metastatic potential of BCCs, but slightly suppressed their tumor growth. RNA sequencing analysis revealed that the suspension state resulted in an acquisition of unique molecular signature enriched in pro-metastatic and tumor-suppressive genes. Specifically, prostaglandin-endoperoxide synthase 2 (*PTGS2*), which encodes protein cyclooxygenase-2 (COX-2), was identified as a highly up-regulated gene in suspension state compared with adherent cultured BCCs. Inhibition of the catalytic activity of COX-2 by celecoxib markedly suppressed suspension-increased migration and invasion of BCCs. In addition, knock-down of COX-2 by siRNA reduced the experimental lung metastasis formation of suspension cultured BCCs, which was associated with a remarkable decrease in retention and survival of BCCs in lungs of mice in the early stage of metastasis. Activation of Ca^{2+}/calcineurin (CaN)/nuclear factor of activated T cells (NFAT) pathway and disruption of cytoskeleton contributed to the COX-2 up-expression by suspension state.

Conclusions: Our results demonstrate that suspension state plays an important role in the metastatic potential of CTCs, and suggest a potential application of COX-2 inhibitor for anti-metastasis.

Key words: suspension state, tumor metastasis, breast cancer, cyclooxygenase-2, cytoskeleton

Introduction

Although major advances have been made in diagnosis and treatment of primary breast cancer, metastasis, typically to bone, lung, liver, and brain, is still the leading reason for mortality of cancer patients. Hematogenous metastasis is the main way of cancer distant metastasis, of which the early step requires tumor cells to detach from the extracellular matrix (ECM) in primary tumor into the bloodstream or lymphatic system and be in a suspension state. Those tumor cells in the blood circulation are called

circulating tumor cells (CTCs). ECM not only supports cell anchorage and maintains tissue integrity, but also broadly impacts cell morphology, cycle control, differentiation and migration depending on ECM stiffness, composition, structure and organization [1-3]. There is increasing evidence that the development of breast tumor is often accompanied by extracellular matrix abnormal deposition, cross-linking and stiffening [4, 5]. Matrix stiffness can regulate the tumorigenicity, proliferation, migration, invasion, epithelial-mesenchymal transition (EMT), as well as drug resistance of breast tumor cells [6-10]. The effect of matrix stiffness on cells mainly works through 1) integrins-mediated kinase signaling [11], and 2) cytoskeleton structure and tension-mediated mechanosensitive transcription factors, such as Yes-associated protein (YAP)/WW domain-containing transcription regulator 1 (TAZ) and TWIST1 [6, 12]. There is no doubt that, once detached from primary tumor, CTCs will lose almost all of the biochemical and biophysical signaling from ECM. In addition, CTCs undergo a dramatic shape change driven by cytoskeletal remodeling. When detaching from ECM, cells lose focal adhesions-mediated anchors and round rapidly, accompanied with a decrease of cytoskeletal tension and degeneration of stress filaments. Cytoskeleton is an indispensable component of force propagation from extracellular to nuclear, in which the force may induce direct stretching of chromatin to regulate gene expression [13, 14]. Cytoskeletal tension itself can be a force stimulus affecting mechanosensitive elements, such as nuclear lamina and the ion channels on the cell membrane [15-17]. Thus, the unique difference in cytoskeletal structure and mechanical characteristic of CTCs from primary tumor cells may affect the signaling pathway and gene expression of CTCs. In fact, the recent application of single-molecule RNA sequencing platform to gene expression identification of CTCs found that CTCs express a set of transcripts involved in the survival and metastatic propensity of CTCs, which were underrepresented in both primary and metastatic tumors [18-21]. Although it has been suggested that a biochemical cue, such as platelet-derived transforming growth factor-β1 (TGF-β1) signaling, might contribute to the distinctive gene expression profile of CTCs [22], the physical characteristics of CTCs also have potential effects on the plasticity of CTCs. Malin et al. [23] reported that suspension state-mediated suppression of extracellular regulated protein kinases (ERK) signaling increased αB-crystallin expression, which facilitated the survival of CTCs and lung metastasis. Based on these studies, we hypothesized that the suspension state, which is an essential feature of CTCs, might provide a signaling platform for efficient metastasis.

In this study, we modeled the suspension state of CTCs by culturing breast cancer cells (BCCs) on low attachment plates to investigate the effect of suspension state on the metastatic potential of BCCs and studied the mechanobiological mechanisms involved. The results provided insights into the roles of suspension state of CTCs in tumor metastasis.

Results

Effects of suspension state on proliferation, survival, migration and invasion of BCCs

After 3 d of suspension culture, BCCs MDA-MB-231 and SK-BR-3 had lower proliferation rates and higher apoptotic levels as compared with the adherent culture group (**Figure 1A-B** and **Figure S1A-B**). Suspension culture also significantly decreased the clone formation ability of MDA-MB-231 cells (**Figure 1C**), but not SK-BR-3 cells (**Figure S1C**). After reattached culture in medium without fetal bovine serum (FBS) for 4 d, most MDA-MB-231 cells from the adherent culture were non-spreading with large numbers of apoptotic bodies/debris (**Figure 1D**). In contrast, most MDA-MB-231 cells from the suspension culture attached well and displayed normal elongated spindle-like morphology. Assays for cell viability confirmed that MDA-MB-231 cells from suspension culture were highly resistant to stress imposed by nutrient deprivation. The same results were observed in SK-BR-3 cells from suspension culture (**Figure S1D**). On the other hand, after reattached culture in medium containing 10% FBS, a modest delay in growth of MDA-MB-231 cells from suspension culture was determined by cell viability assays (**Figure 1E**). In addition, suspension culture markedly increased the migration ability of BCCs, both MDA-MB-231 cells and SK-BR-3 cells, in a time-dependent way (**Figure 1F** and **Figure S1E**). Moreover, compared with the adherent culture BCCs, BCCs from suspension culture had a higher ability to invade (**Figure 1G** and **Figure S1F**). These results suggested that, although suspension state harmed the proliferation of BCCs, suspension state promoted survival under hostile conditions and enhanced the migration and invasion ability of BCCs.

Suspension state primes BCCs for metastasis

To explore effects of suspension state on tumor growth and metastasis, a xenograft model and an experimental lung metastasis model were made in female nude mice (**Figure 2A**). The tumors formed by MDA-MB-231 cells from suspension culture for 3 d were significantly smaller in volume (**Figure 2B**) and lower in weight (**Figure 2C**) relative to those formed

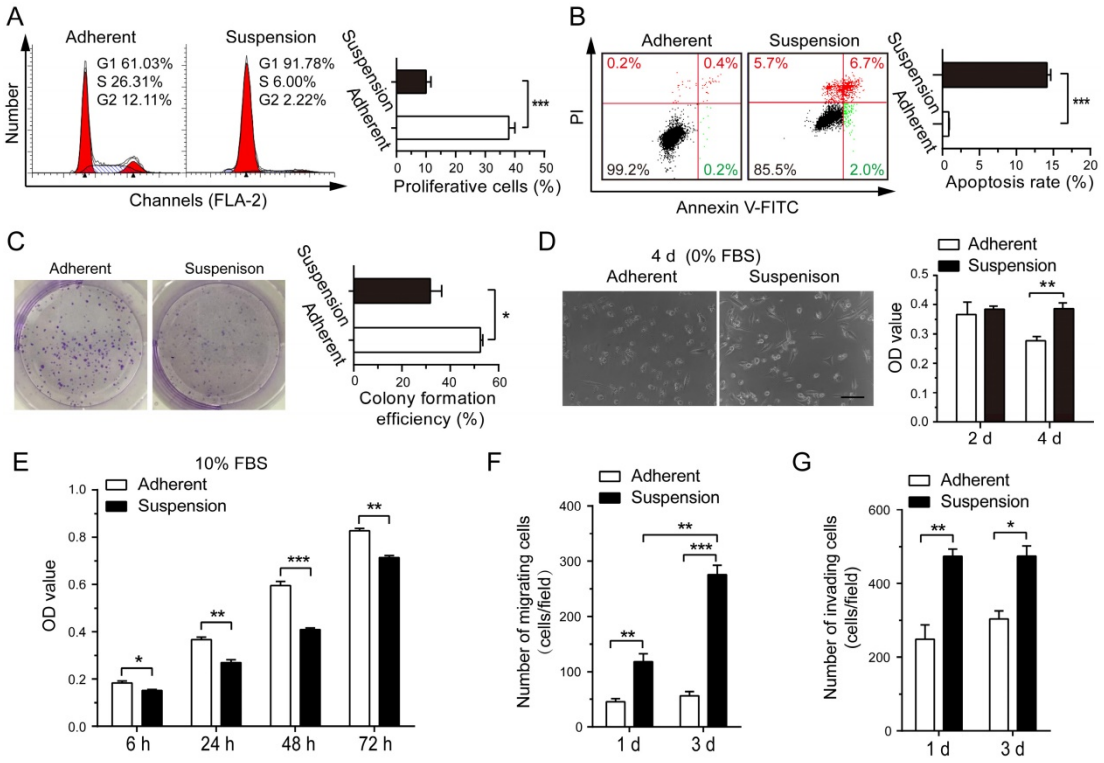

Figure 1. Effects of suspension state on proliferation, apoptosis, colony formation, survival, migration and invasion ability of MDA-MB-231 cells. MDA-MB-231 cells were cultured under suspension state at a density of 2×10^5 cells/mL or conventional adherent condition for 3 d. **(A)** Cell cycle analysis and **(B)** cell apoptosis analysis by flow cytometry. Representative plots are displayed. **(C)** Adherent or suspension-cultured MDA-MB-231 cells were seeded at a density of 500 cells/well for clone formation assays. Representative crystal violet staining of clone formation is shown. MDA-MB-231 cells from adherent culture and suspension culture were seeded and cultured in DMEM medium without FBS **(D)** or with 10% FBS **(E)**. Phase contrast micrographs of MDA-MB-231 cells cultured for 4 d without FBS are given (scale bar = 50 μm). MTS assays were used to measure cell viability. **(F)** Migration assays and **(G)** invasion assays of MDA-MB-231 cells after adherent or suspension culture for 1 d and 3 d. Values are presented as mean ± SE (n=3). *P< 0.05; **P< 0.01; ***P< 0.001.

by adherent culture cells. However, the lung metastatic nodules formed by injecting mice with suspension MDA-MB-231 cells were remarkably increased from 6.5 (± 0.9, SE)/lung in the adherent culture group to 53.8 (± 7.0, SE)/lung in the suspension culture group (**Figure 2D-E**). As a result, the weight of lungs in the suspension culture group was markedly greater than that in the adherent culture group (**Figure 2F**). The hematoxylin-eosin (H-E) staining of lung sections showed that the suspension culture group had more lung metastasis and larger metastatic focus than the adherent culture group (**Figure 2G**). Overall, these results indicated that the suspension state of BCCs exerted tumor-suppressive effects and pro-metastatic effects.

Suspension state induces pro-metastatic genes expression in BCCs reversibly

To elucidate the potential mechanisms underlying the functional effects of suspension state, MDA-MB-231 cells from suspension and adherent culture were subjected to RNA sequencing. The analysis revealed that 254 genes were up-regulated and 190 genes were down-regulated by at least four-fold in suspension culture cells relative to adherent culture cells (**Figure 3A** and **Dataset S1**). Differentially expressed genes were significantly enriched in gene ontology (GO) terms associated with immune response, cell cycle, apoptotic, extracellular matrix, cell adhesion, cell migration, metallopeptidase activity, angiogenesis, among numerous other terms (**Figure 3B**). As anticipated, almost all genes enriched in cell cycle were down-regulated by suspension culture (**Figure 3C**). On the other hand, suspension state up-regulated most genes enriched in GO term related to regulation of apoptotic process, extracellular matrix, cell adhesion, cells migration, metallopeptidase activity and angiogenesis. qRT-PCR assays validated robust increases in expression of pro-metastatic genes associated with extracellular matrix *fibronectin 1* (*FN1*) and *LOX*, cell adhesion molecules including *mucin1* (*MUC1*), *SELPLG* and *intercellular adhesion molecule* (*ICAM-1*), as well as drug resistance protein *ABCC3* and TGF-β signaling pathway *TGFBR2* and *TGFB1* (**Figure S2A**). Interestingly, up-expression of those genes induced by suspension state was time-dependent and reversible. Specifically, after reattached culture for 48 h, up-expression of those genes was suppressed to the level of adherent culture cells. Western blotting assays showed the consistent finding in protein levels of FN, MUC1 and ICAM-1 (**Figure S2B**). Taken together,

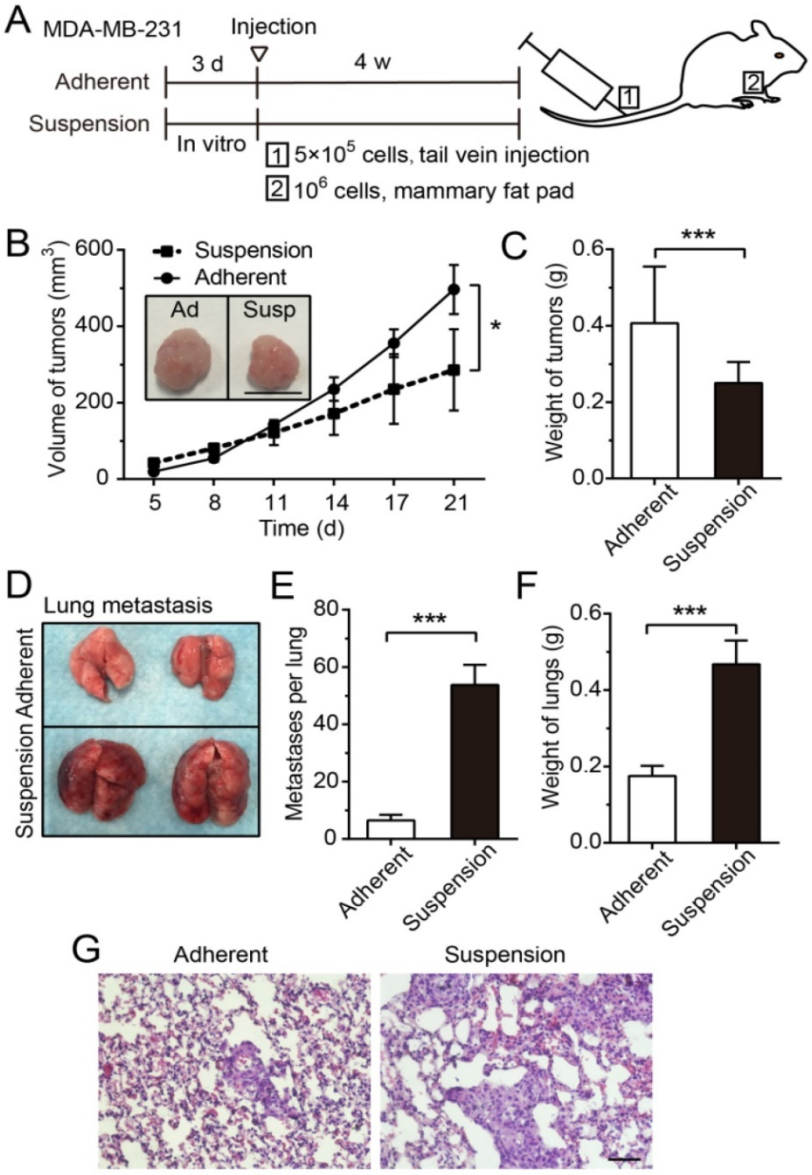

Figure 2. Suspension state of MDA-MB-231 cells suppressed tumor growth, but promoted lung metastasis. (A) Schematic of the xenograft model and experimental metastasis model. **(B)** Measurement of tumor volume in the xenograft model. Values are presented as mean ± SE (n=3). *P< 0.05 (paired t-test). Representative images of tumors at 21 d after injection (scale bar = 1 cm). Ad: adherent; Susp: suspension. **(C)** Measurement of tumor weight in the xenograft model. Values are presented as mean ± SE (n=3). *P< 0.05 (paired t-test). **(D)** For the experimental metastasis model, adherent or suspension MDA-MB-231 cells were injected via tail vein. Representative images of lungs at 28 d after injection. **(E)** Counting of metastases on mouse lungs. Values are presented as mean ± SE (n=4). ***P< 0.001. **(F)** Measurement of lung weight in the experimental lung metastasis model. Values are presented as mean ± SE (n=4). ***P< 0.001. **(G)** Representative images of H-E staining of lung metastasis (scale bar = 50 μm).

suspension state promoted a unique BCCs gene signature involved in metastasis, suggesting that suspension state-promoted metastasis was a result of multiple factors.

Suspension-induced cyclooxygenase-2 (COX-2) expression promotes metastasis *in vitro* and *in vivo*

We noted that prostaglandin-endoperoxide synthase 2 (*PTGS2*) gene, which encodes protein COX-2 and is associated with regulation of apoptotic process and cell migration, was highly up-regulated by suspension culture in MDA-MB-231 cells (**Figure 3B**). qRT-PCR assays and western blotting assays showed that the mRNA level and protein level of COX-2 were progressively increased in suspension state from the first few hours to 72 h and gradually decreased to the basic levels after suspension cells reattached (**Figure 4A-B**). Suspension state also up-regulated COX-2 in SK-BR-3 cells reversibly (**Figure 4C**). To define the functional consequences of COX-2 expression in suspension-cultured BCCs, we first investigated the effects of COX-2 on migration and invasion *in vitro* by using COX-2 inhibitor celecoxib (CXB). BCCs were cultured in suspension condition for 2 d, then treated with CXB for 1 d with or without new medium and prostaglandin E_2 (PGE_2). Under our experimental condition, CXB had no

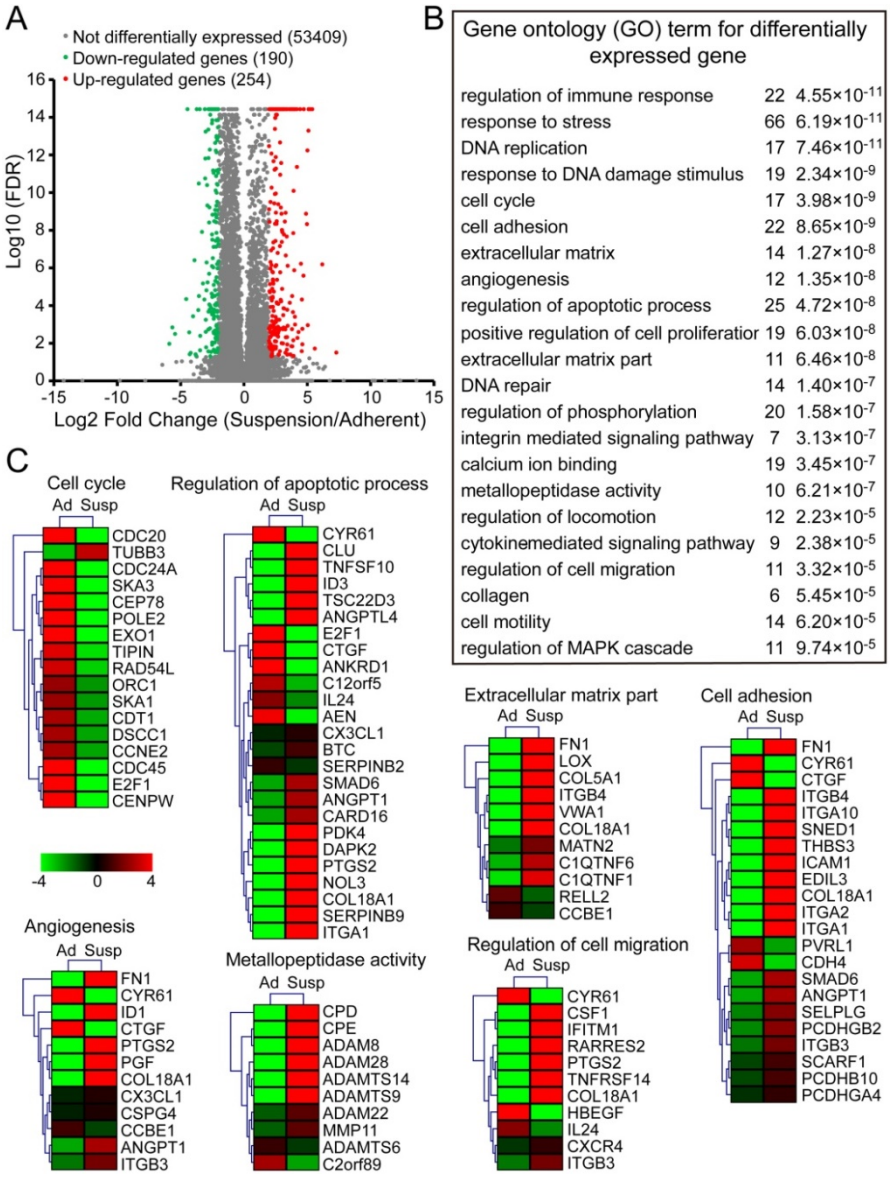

Figure 3. RNA sequencing analysis of suspension cells and adherent cells. Total RNAs of MDA-MB-231 cells after adherent or suspension culture for 3 d were isolated for sequencing. **(A)** Scatter plots of differently expressed genes between adherent and suspension MDA-MB-231 cells (false discovery rate (FDR) < 0.05). Plots highlighted with red and orange represent up-regulated genes in suspension cells, relative to adherent cells, while green and blue plots are down-regulated genes. **(B)** Gene ontology (GO) term ($P < 10^{-4}$) for differently expressed genes (change more than four-fold) related to tumor cell survival and metastasis. **(C)** Expression heat map of genes in the set of some GO terms selected from (B). Scale in log 10 (FPKM). FPKM: fragments per kilobase of exon model per million mapped reads; Ad: adherent; Susp: suspension.

significant effects on the migration and invasion of MDA-MB-231 cells and SK-BR-3 cells without change of medium (**Figure 4D-G**). In contrast, CXB in new medium without PGE_2 markedly decreased the migration and invasion of BCCs. Extra PGE_2 significantly reactivated cell invasion, but not migration. These results indicated that the suspension state promoted BCCs migration and invasion due to the up-expression of COX-2, *via* PGE_2-mediated signaling to a certain extent.

Subsequently, we evaluated the effect of COX-2 on metastasis of suspension MDA-MB-231 cells *in vivo*. GFP-expressing MDA-MB-231 cells were transfected with COX-2-targeted siRNA (si-COX-2) or control siRNA (si-Ctrl) and cultured in adherent or suspension condition for 3 d, then subjected to tail vein injection (**Figure 5A** and **Figure S3A**). Transfection of COX-2 siRNA led to a >80% reduction in the expression of COX-2 induced by the suspension state (**Figure S3B-C**). After 28 d, the lung metastatic nodules formed by injecting mice with suspension MDA-MB-231 cells were clearly repressed by si-COX-2 (**Figure 5B**). The weight of lungs was also dramatically decreased about 50% by silencing COX-2 in suspension MDA-MB-231 cells (**Figure 5C**). The H-E staining of lung sections showed that silencing COX-2 in suspension MDA-MB-231 cells resulted in less lung metastasis and smaller metastatic focus relative to the si-Ctrl group (**Figure 5D**).

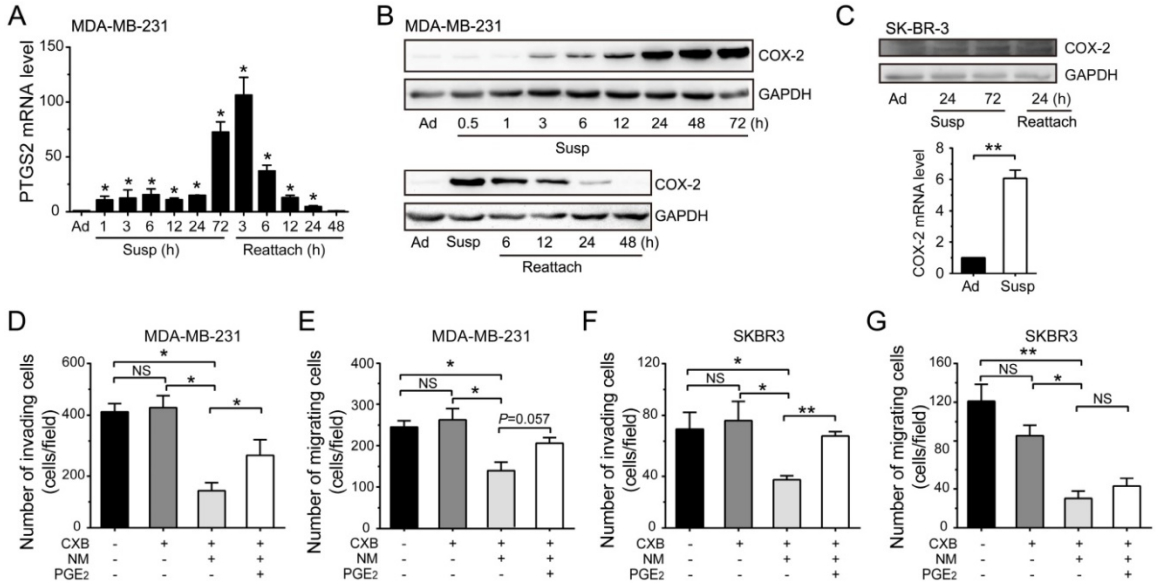

Figure 4. Suspension state induced COX-2 up-regulation to promote the migration and invasion abilities of BCCs. (A) Detection of *PTGS2* level by qRT-PCR in suspension (Susp) and reattached (Reattach) MDA-MB-231 cells. **(B)** Detection of COX-2 protein level by western blotting in suspension and reattached MDA-MB-231 cells. GAPDH was used as loading control. **(C)** Protein level and mRNA level of COX-2 in SK-BR-3 cells were detected. Invasion and migration assays for MDA-MB-231 **(D-E)** and SK-BR-3 cells **(F-G)**. BCCs were suspension cultured for 2 d, then cultured for another 1 d with CXB and PGE_2 in new medium (NM) or not. Values are presented as mean ± SE (n=3). *P< 0.05; **P< 0.01; NS, not significant.

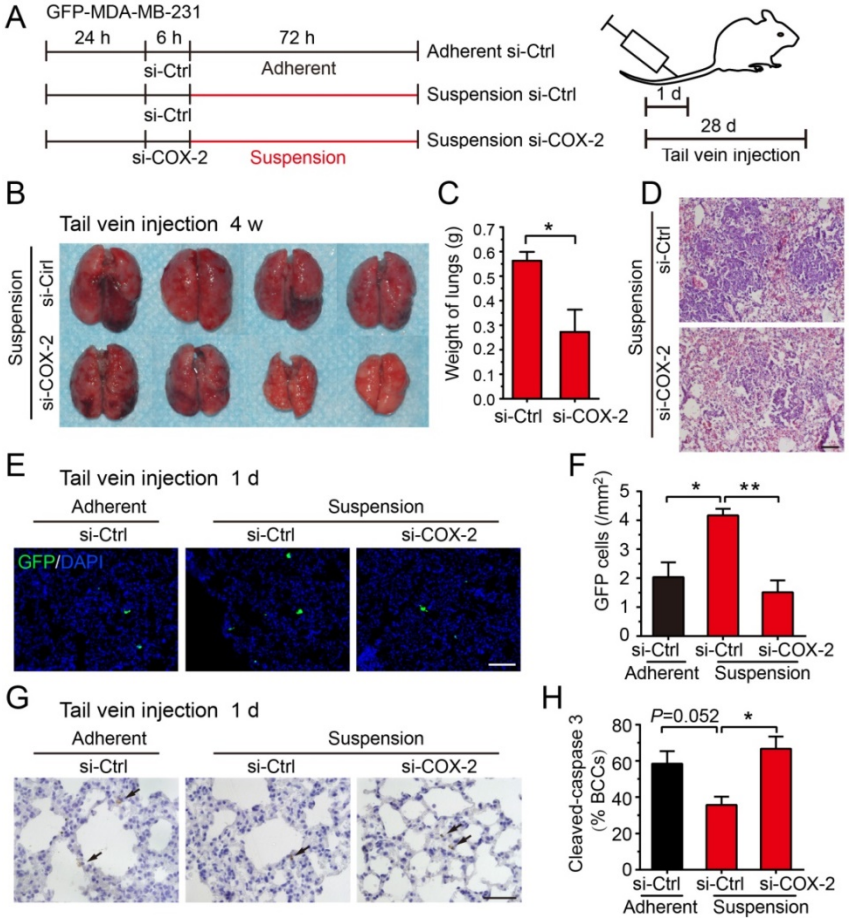

Figure 5. Knockdown of COX-2 inhibited suspension-promoted lung metastasis by decreasing cancer cell capture in lung and increasing resistance to apoptosis. (A) Schematic of experimental lung metastasis of MDA-MB-231 cells with COX-2 knockdown. Adherent or suspension-cultured GFP-MDA-MB-231 cells with COX-2 knockdown (si-COX-2) or not (si-Ctrl) were injected *via* tail vein. **(B)** Images of mouse lungs at 28 d after injection of suspension cells with COX-2 knockdown or not. **(C)** Measurement of lung weights. Values are presented as mean ± SE (n=4). *P< 0.05. **(D)** Representative images of H-E staining of lungs metastasis (scale bar = 50 μm). **(E)** Representative images of GFP-positive cells in sections of mouse lungs 24 h after injection with adherent si-Ctrl cells, suspension si-Ctrl or suspension si-COX-2 cells. Nuclei were stained with DAPI (scale bar = 50 μm). **(F)** Graph showing the number of GFP-positive cells. Values are presented as mean ± SE (n=3). *P< 0.05; **P< 0.01. **(G)** Immunohistochemical staining of cleaved caspase 3 in tumor cells of mouse lungs 24 h after injection with BCCs (scale bar = 50 μm). **(H)** Graph showing the mean percentage of cleaved caspase 3-positive cells. Values are presented as mean ± SE (n=3). *P< 0.05; **P< 0.01.

Up-expression of COX-2 could not be detected in tumors and lung metastases driven by suspension MDA-MB-231 cells, suggesting that the up-regulation of COX-2 was abolished after the suspension state disappeared *in vivo* (**Figure S4**). Thus, we postulated that COX-2 played a critical role in the early stage of suspension-promoted metastasis. To verify this supposition, GFP-positive (viable cells) and cleaved caspase 3-positive (apoptotic cells) MDA-MB-231 cells were counted in lungs sections 1 d after tail vein injection. GFP-positive cells in lungs of the mice injected with suspension MDA-MB-231 cells were about 2-fold relative to that of the adherent culture group (**Figure 5E-F**). Silencing COX-2 in suspension-cultured MDA-MB-231 cells significantly decreased lung-captured cancer cells to the level seen in adherent cultured cells. There was no significant difference of the number of apoptotic tumor cells in lungs among the three groups, i.e., adherent-cultured cells, suspension-cultured cells, and suspension-cultured cells with COX-2 silencing (**Figure 5G**). As the suspension-cultured cells group had the largest number of viable tumor cells in lungs, the ratio of apoptotic tumor cells of this group was minimum (**Figure 5H**). Coinciding with the *in vivo* result, silencing COX-2 greatly decreased cell viability and increased apoptosis (**Figure S3D-E**), and slightly decreased clone formation of suspension MDA-MB-231 cells *in vitro* (**Figure S3F**). Overall, the COX-2-induced by suspension state contributed to metastasis *via* increasing the capture and survival of tumor cells in lungs.

Suspension state causes Ca^{2+}/calcineurin (CaN)/nuclear factor of activated T cells (NFAT) activation and cytoskeleton change to contribute to COX-2 up-expression

The COX-2 expression induced by mechanical stimulations, such as flow shear stress, compression and mechanical stretching, is always associated with activation of Ca^{2+}/CaN/NFAT [24, 25]. To investigate whether Ca^{2+}/CaN/NFAT signaling was involved in the up-regulation of COX-2 in suspension BCCs, we first compared the intracellular calcium levels in adherent cells and suspension cells by using Fluo 3 probe. As shown in **Figure 6A**, the Ca^{2+} level was increased in suspension-cultured MDA-MB-231 cells. Calcium channel inhibitor $LaCl_3$ and CaN inhibitor cyclosporine A (CsA) led to about 50% reduction in the protein level of COX-2 in suspension-cultured MDA-MB-231 cells (**Figure 6B-C**). Subsequently, we

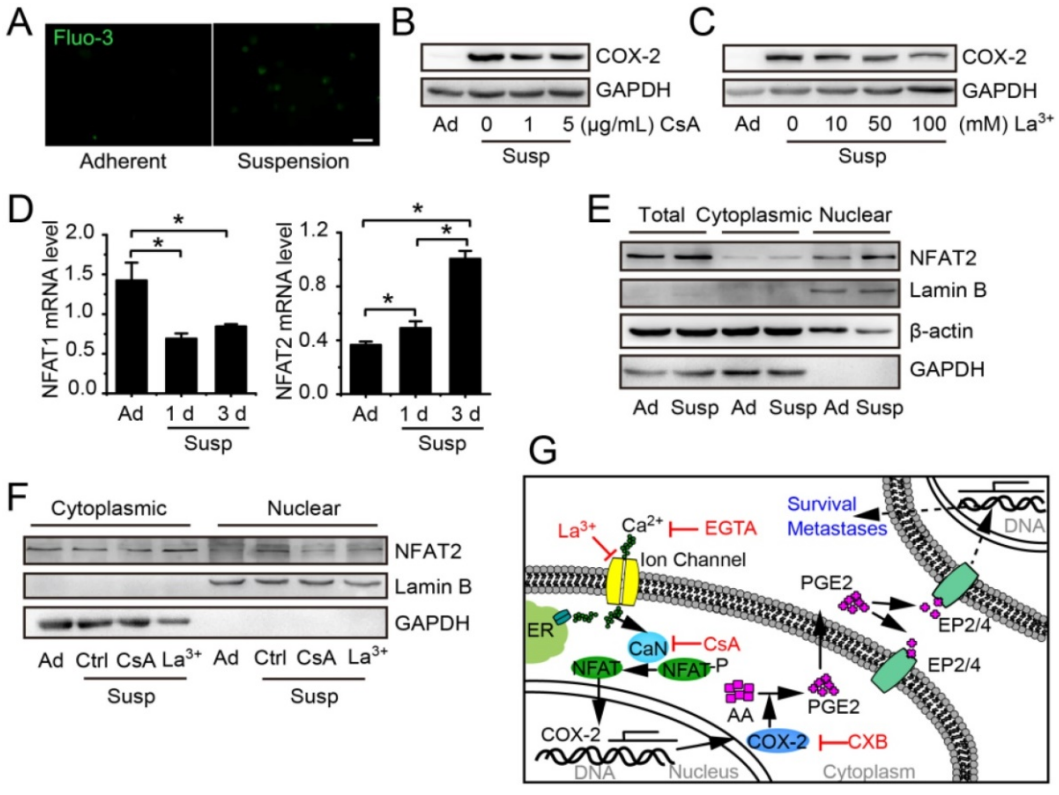

Figure 6. Suspension state activated Ca^{2+}/CaN/NFAT2 signaling contributing to COX-2 upregulation. (A) Cytosolic Ca^{2+} levels were estimated by Fluo-3/AM in adherent or suspension cultured MDA-MB-231 cells (scale bar = 20 μm). COX-2 protein level in suspension cultured MDA-MB-231 cells with Ca^{2+}/CaN signing inhibitor CsA **(B)** or $LaCl_3$ **(C)**. GAPDH was used as loading control. **(D)** Detection of NFAT1 and NFAT2 mRNA levels in adherent or suspension MDA-MB-231 cells. Values are presented as mean ± SE (n=3). *P< 0.05. **(E)** Detection of total protein expression and nuclear accumulation of NFAT2 in adherent or suspension MDA-MB-231 cells. **(F)** Detection of nuclear NFAT2 protein levels in suspension cells with CsA (1 μg/mL) or $LaCl_3$ (100 μM).GAPDH was used as loading control for total and cytoplasmic protein. Lamin B was used as loading control for nuclear protein. **(G)** Schematic of Ca^{2+}/CaN/NFAT2 signaling contributing to COX-2 expression. Ad: adherent; Susp: suspension; Ctrl: control.

examined the expression and nuclear accumulation of NFAT. Suspension state decreased the mRNA level of NFAT1, but increased the mRNA level of NFAT2 (**Figure 6D**) as well as the total protein level and nuclear accumulation of NFAT2 (**Figure 6E**). Inhibition of Ca^{2+}/CaN by $LaCl_3$ or CsA clearly decreased the protein level of NFAT2 in nuclei (**Figure 6F**). Taken together, the activation of Ca^{2+}/CaN/NFAT2 signaling contributed to COX-2 up-expression by the suspension state (**Figure 6G**).

It has been reported that decreasing matrix stiffness strongly induces expression of COX-2 and that blocking ROCK with Y27632 increases COX-2 expression in fibroblast cells [26]. Suspension state is similar to the extreme case of soft matrix. Thus, we hypothesized that cytoskeleton organization and cell contraction might play a role in suspension-induced COX-2 expression. Decreasing matrix stiffness suppressed stress fiber organization and cell spreading of MDA-MB-231 cells (**Figure 7A**). Cytochalasin D (CytoD) disrupted the cytoskeleton integrity and formation of stress fibers in MDA-MB-231 cells planted on tissue culture polystyrene (TCPS) plates (**Figure 7B**). Decreasing matrix stiffness significantly induced the expression of COX-2 in MDA-MB-231 cells (**Figure 7C**). Moreover, cytoskeleton disruption by CytoD strongly increased the mRNA level of COX-2 across the entire range of matrix stiffness tested (**Figure 7C**). Interestingly, suspension-induced *FN1*, *LOX* and *ABCC3* also responded to matrix stiffness (**Figure S5A-C**). Western blotting showed that the protein level of COX-2 was increased by CytoD treatment both in adherent-cultured and suspension-cultured MDA-MB-231 cells, but not by inhibition of cell contraction with Y27632 (**Figure 7D**). Interestingly, cytoskeleton disruption by CytoD also could increase the total protein level and nuclear accumulation of NFAT2 in adherent MDA-MB-231 cells (**Figure 7E**). To confirm whether the COX-2 induced by cytoskeleton disruption was related to Ca^{2+}/CaN/NFAT signaling, the intracellular Ca^{2+} level was detected in MDA-MB-231 cells cultured on polyacrylamide gel with different stiffness. The intracellular Ca^{2+} levels were high in cells cultured on 5 kPa and 20 kPa gel, without a significant difference,

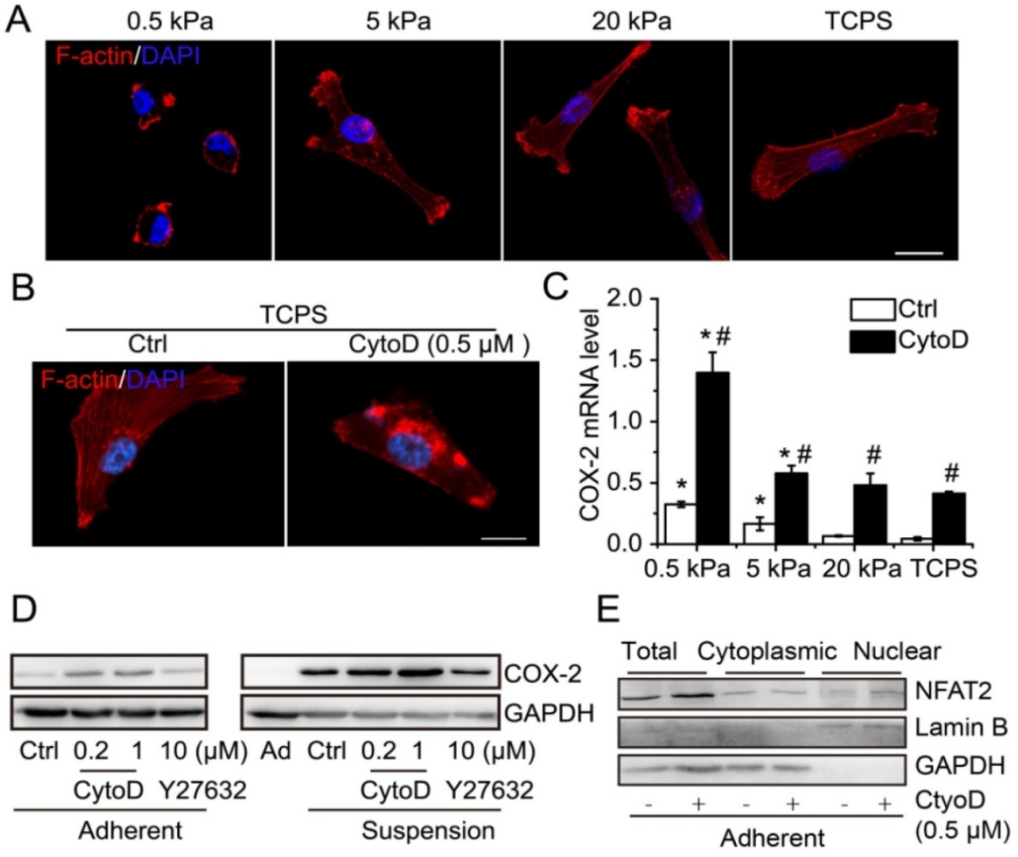

Figure 7. Cytoskeleton disruption contributed to COX-2 expression. (A) Immunofluorescence microscopy showed F-actin staining with phalloidin of MDA-MB-231 cells cultured on PAAs with different stiffness and TCPS. **(B)** F-actin staining with phalloidin in MDA-MB-231 cells with cytoskeleton disruption by CytoD. Nuclei were stained with DAPI (scale bar = 10 μm). **(C)** Detection of COX-2 mRNA expression in MDA-MB-231 cells cultured on matrix with different stiffness with CytoD, or not. Values are presented as mean ± SE (n=3). *P< 0.05, relative to TCPS with CytoD, or not. #P< 0.05, relative to control on matrix with the same stiffness. **(D)** COX-2 protein expression in adherent and suspension cultured MDA-MB-231 cells with CytoD or ROCK inhibitor Y27632. GAPDH was used as loading control. **(E)** Detection of total protein level and nuclear accumulation of NFAT2 in MDA-MB-231 cells when cytoskeleton was disrupted by CytoD (0.5 μM). GAPDH was used as loading control for total and cytoplasmic protein. Lamin B was used as loading control for nuclear protein. Ad: adherent; Ctrl: control.

and were low in cells cultured on 0.5 kPa gel and TCPS, again without significant difference (**Figure S5D-F**). The results indicated that COX-2 expression induced by cytoskeleton disruption was independent of Ca^{2+}/CaN/NFAT signaling. Overall, the suspension state induced COX-2 expression by activation of Ca^{2+}/CaN/NFAT signaling and cytoskeleton disruption.

Discussion

The suspension state of CTCs is an inevitable stage in tumor distant metastasis, not only for CTCs, but also for disseminated tumor cells in malignant pleural effusion. In the past, suspension state was considered as being disadvantageous for CTCs due to apoptotic induction and growth suppression. In recent years, the other side of suspension state in CTCs has gradually been noticed. Our previous research proved that suspension state promoted the reattachment of BCCs by up-regulating lamin A/C *via* cytoskeleton disruption [27]. In addition, a study showed that suspension state of cancer cells induced microtubule-based microtentacles to promote reattachment *in vitro* and metastasis *in vivo* [28].Our present research indicated that the suspension state was not beneficial for the clone formation of MDA-MB-231 cells and delayed proliferation after reattachment under nutritionally adequate condition, which might be due to partial apoptosis and cycle arrest. These effects significantly suppressed the potential of suspension-cultured MDA-MB-231 cells to form tumors in immunodeficient nude mice. It's interesting that suspension state had no effect on the clone formation of SK-BR-3 cells, which might be due to the smaller impact on cell cycle and apoptosis compared with MDA-MB-231 cells. The positive expression of human epidermal growth factor receptor 2 (Her2) on SK-BR-3 cells, while MDA-MB-231 cells are Her2-negative, might be the deeper reason, because Her2 could promote the proliferation and anoikis resistance of BCCs [29]. On the other hand, our finding that suspension-preconditioned BCCs displayed a robust ability to survive in conditions with nutrient deficiency indicates that the suspension state might promote the survival of CTCs captured by target organs. Moreover, the suspension state improved the ability of migration and invasion of BCCs, which might contribute to the extravasation of CTCs, escaping from the circulatory system to avoid damage from flow shear stress and to form metastases. Although suspension-cultured BCCs had partial apoptosis and cycle arrest, more of these cells could extravasate and survive to form metastases than adherent-cultured BCCs. Consequently, the results indicate that the suspension state resulted in a marked increase in lung metastasis in immunodeficient nude mice.

Using RNA sequencing to analyze the molecular mechanisms by which suspension state modulates the metastatic potential of BCCs, we found 444 differentially expressed genes with at least a four-fold change. Conforming to the growth suppression effect of suspension state, cell cycle associated genes were down-regulated broadly. A similar result was obtained in Bartosh's study [30]. In addition, suspension state induced expression of apoptotic regulation-associated genes, such as *PTGS2*, *ITGA1*, *ID3*, *CLU*, *ANGPTL4*, *ANGPT1* (**Figure 3C**), all of which contribute to anoikis resistance [31-35]. It has been reported that suspension state could induce αB-crystallin expression to promote anoikis resistance and lung metastasis of MDA-MB-435 BCCs [23]. However, in this study, the up-expression of αB-crystallin couldn't be detected in the suspension-cultured MDA-MB-231 cells by RNA sequencing (data not shown). The expression of anoikis resistance-related genes might be the reason why apoptosis happened only in a small part of the suspension BCCs, although it is unclear whether the normal epithelial cells will up-regulate those anti-apoptosis genes under suspension state. According to previous studies, after matrix detachment, normal epithelial cells tend to undergo apoptosis induced by disruption of integrin-mediated cell survival signals, while tumor cells could overcome anoikis due to genetic abnormalities (e.g., neurotrophic receptor tyrosine kinase B (TrkB), B-Raf proto-oncogene (B-RAF)) [36, 37]. In recent years, several studies have also shown that biochemistry cues like TGF-β1 derived by platelets and physical characteristics of CTCs, such as multicellular clusters, contributed to the survival of CTCs [22, 38]. Our present research revealed that the up-regulation of anoikis resistance-related genes induced by suspension state might be another mechanism for CTCs survival. In addition, consistent with our previous results that suspension state improved the adhesion ability of BCCs [27], suspension state resulted in up-regulated expression of genes critical for cell adhesion, including *ICAM-1*, *SELPLG*, *ITGB4*, *ITGB3*, *ITGBA1*, *ITGBA2* (**Figure 3C**). Suspension state also increased the expression of migration (*CSF1*, *PTGS2*, *CXCR4*, *ITGB3*) and ECM degradation (*CPD*, *CPE*, *MMP11*, *ADAM* family) related genes, which might contribute to the promotion of migration and invasion of BCCs in suspension. In addition, ECM genes (*FN*, *LOX*, *COL5A1*, *COL18A1*, *ITGB4*) were up-regulated in suspended BCCs. Consistent with the above results, significant enrichment for ECM genes was also confirmed in CTCs from pancreatic and

breast cancers by single-molecule RNA sequencing platform [18, 20]. Our results indicated that suspension state might be the potential reason for CTCs-specific gene-expression patterns compared with primary tumor. While the regulation of all genes was time-dependent, there were differences in their response time. These results indicated that some genes (*PTGS2*, *MUC1*) up-regulated in 1 h might be suspension state sensitive, while others might be induced by signals mediated by suspension-sensitive genes rather than being directly modulated by suspension state.

Among those suspension-sensitive genes, *PTGS2*, encoding COX-2, was one of the most up-regulated genes and induced in 1 h. COX-2 is an inducible enzyme, often overexpressed in breast, colorectal, lung and pancreatic cancers and melanoma, and is associated with poor survival [39-43]. COX-2 converts arachidonic acid to prostaglandins, including PGE_2 associated with enhancement of cancer cell survival, growth, migration, invasion, stem cells-like property, angiogenesis, and immunosuppression [44]. COX-2 inhibitors, e.g., CXB and aspirin, show potentials for cancer prevention [45], and synergistic effect with anti-PD-1 blockade in preclinical models [46]. As expected, we demonstrated that the up-regulation of COX-2 and synthesis of PGE_2 played important roles in suspension-promoted migration and invasion of BCCs. In addition, reduction of suspension-induced COX-2 expression by siRNA significantly increased the apoptosis of suspended BCCs. The increased migration and invasion abilities of suspended BCCs, together with their increased apoptotic resistance, may underlie their dramatically enhanced metastatic potential. Consequently, it was found that the suspension state resulted in a remarkable increase in retention and survival of BCCs in lungs of mice in the early stage of metastases formation, which could be suppressed by silencing the expression of suspension-induced COX-2 in BCCs. Ultimately, suspension-promoted metastasis formation was reduced. In general, our study suggests that suspension state can rapidly induce COX-2 expression to enhance the metastatic potential of BCCs.

The NFAT family of transcription factor is composed of four Ca^{2+}-regulated members (NFAT1-4) and one osmotic stress-regulated member (NFAT5) [47, 48]. Activation of CaN by Ca^{2+} catalyzes NFAT dephosphorylation, leading to NFAT nuclear translocation to regulate gene transcription. Previous results showed that the CaN/NFAT 1 and NFAT 2 pathway is activated in breast cancers and is essential to the tumorigenic and metastatic potential of a mammary tumor cell line [49]. Notably, COX-2, as a target gene of NFAT, could be induced by NFAT to synthesize PGE_2, thus promoting BCCs invasion [50]. We found that the suspension state of BCCs activated Ca^{2+}/CaN/NFAT2 to contribute to COX-2 up-regulation. Inhibition of calcium ion channel activity by $LaCl_3$ and inhibition of CaN by CsA both abolished suspension-induced NFAT nuclear accumulation, but could not inhibit completely the suspension-induced COX-2 expression, suggesting other mechanisms are involved in COX-2 up-regulation.

It has been reported that decreasing matrix stiffness increased the expression of COX-2 in several types of cells [26]. In this study, similar results were found in MDA-MB-231 cells. Interestingly, decreasing matrix stiffness also up-regulated genes *FN*, *LOX*, *ABCC3*, all of which were inducible under suspension condition. In spite of the regulation of intracellular Ca^{2+} level by matrix stiffness, intracellular Ca^{2+} levels had no obvious correlation with the expression levels of these genes in MDA-MB-231 cells cultured on matrix with different stiffness. These results indicate that soft matrix could induce suspension-sensitive genes expression in a Ca^{2+}-independent way. Although cells under suspension state are not the same as those on soft matrix, their cytoskeleton structure and shape are similar. The cells on soft matrix could not spread well, with a disorder in actin cytoskeleton and a decrease in cell tension. Furthermore, we have demonstrated that disruption of actin cytoskeleton by CytoD induced COX-2 expression in MDA-MB-231 cells cultured on matrix with different stiffness and under suspension condition. However, inhibition of actin cytoskeleton contraction by Y27632 had no significant effect on COX-2 expression in MDA-MB-231 cells, which is different from the previous study on human lung fibroblast [26]. Our recent research showed that disruption of actin cytoskeleton in adherent BCCs resulted in nucleus shrinking from a flat-shape, with obvious reduction in nuclear areas and roundness, but inhibition of actin cytoskeleton contraction had no similar effect on the nucleus [27]. Together with the fact that tumor cells cultured under suspension state and on soft matrix also had shrunken nuclei, we proposed that the expression of suspension-sensitive genes, such as COX-2, is related to nuclear deformation induced by cytoskeleton disruption. This notion is supported by recent research that nuclear deformation may immediately cause stretching or compressing of chromatin to facilitate gene transcription [14, 51]. Tensegrity theory suggests that the cell is a prestressed self-balancing structure, consisting of tension-generating elements and compression-bearing elements, and change of local

stress will result in an overall structural response until a new equilibrium is obtained [52, 53]. During matrix detachment, the nucleus, as the hardest and largest organelle in cells, is bound to change its structure and force status, not just shape, such as increasing lamin A/C accumulation [27]. It remains to be elucidated whether those changes in the nuclei of suspended cells play a critical role in the expression of suspension-sensitive genes.

Overall, our results indicate that the suspension state of BCCs promotes metastatic potential by enhancing migration, invasion and survival ability *via* inducing a specific gene expression pattern. The cytoskeleton state and activation of Ca^{2+}/CaN/NFAT are responsible for the up-regulation of COX-2, which plays an important role in suspension-promoted metastasis. The results of this study are helpful in understanding the plasticity of CTCs and the importance of suspension mechanical state in CTC metastasis, and provide a theoretical basis for the anti-metastasis function of COX-2-specific inhibitor.

Methods

Reagents

CytoD was purchased from Millipore (250255, Billerica, USA). Y27632 (S1049), CsA (S1514) and CXB (S1261) were purchased from Selleck (Washington, USA). $LaCl_3$ was purchased from Sigma-Aldrich (449830, Saint Louis, USA). PGE_2 was bought from Peprotech (3632464, New Jersey, USA).

Cell lines and culture

Human BCCs SK-BR-3 and MDA-MB-231 were purchased from the Type Culture Collection of the Chinese Academy of Sciences, Shanghai, China. SK-BR-3 and MDA-MB-231 were cultured in high-glucose DMEM medium (12800-017, Gibco, USA) with 10% FBS (TBD21HY, TBD science, Tianjing, China), 100 units/mL penicillin/ streptomycin, 2 mM L-glutamine (G8540, Sigma, Saint Louis, USA), 26 mM $NaHCO_3$ in a humidified 95% air/5% CO_2 environment at 37 ^oC. Modified from previous research [54], 1 mL of poly (2-hydroxyethyl methacrylate) (Poly-HEMA; P3932, Sigma,Saint Louis, USA) solution (100 mg/mL, dissolved in 95% ethanol) was added into six-well plates and filled the bottom of the culture plates. Excess liquid was sucked away and the six-well plates were placed under sterile condition in a laminar flow hood to dry. The Poly-HEMA-treated six-well plates were washed with phosphate buffer solution (PBS).BCCs were seeded at 5×10^4 cells/mL in Poly-HEMA-treated 6-well plates with complete medium. Conventional adherent culture BCCs were used as the control.

Cell proliferation, cell survival, cell cycle and apoptosis assays

Breast cancer cells SK-BR-3 and MDA-MB-231 cells were cultured in suspension or adherent condition for 3 d. Cells were collected and re-suspended. For cell proliferation assays, 5×10^3 cells were seeded in 96-well plates with 10% FBS. After 3 h, 24 h, 48 h and 72 h, 100 μL new medium with 10 μL MTS (G5421, Promega, Madison, USA) was added into each well. The absorbance at 490 nm was measured. For cell survival assays under nutrient deficiency condition, 1×10^4 cells were seeded in 96-well plates without FBS and cultured for 4 d. The cell activity was detected using MTS assay. For cell cycle profiling, Cell Cycle Analysis Kit (C1052, Beyotime, Beijing, Shanghai, China) was used according to the manufacturer's protocol. In brief, cells were collected and fixed overnight with 70% ethanol at 4 ^oC. Cells were suspended and incubated in PBS containing propidium iodide (PI) and RNAase at 37 ^oC for 30 min. Then, the stained cells were analyzed by BD FACS Calibur Flow Cytometer. For apoptosis assays, cells were stained with Annexin V and PI using the Annexin V-FITC/PI apoptosis assay kit (FAK015.60, Neobioscience, Shenzhen, China), then analyzed by flow cytometry.

Clone formation assays

SK-BR-3 and MDA-MB-231 cells were cultured in suspension or adherent condition for 3 d. Then, cells were seeded at a density of 500 cells/well for MDA-MB-231 cells and 400 cells/well for SK-BR-3 cells in 6-well plates and cultured for 7 d. Cell clones were stained with crystal violet and were counted.

Migration and invasion assays

SK-BR-3 and MDA-MB-231 cells were cultured in suspension or adherent condition for 1 d and 3 d. In some assays, MDA-MB-231 cells were cultured in suspension for 2 d, then treated with CXB (1 μM) for 1 d with or without new medium and PGE_2 (50 ng/mL).Cells were collected and re-suspended. For migration assays, 2.5×10^4 cells in 200 μL DMEM medium without FBS were added into the upper chamber of Transwell plates (8 μm, 24-well plates) and 600 μL DMEM medium with 10% FBS were added into the lower chamber. After 6 h, cells in the upper chamber were removed and cells under the membrane of Transwell®plates were fixed and stained with DAPI. Randomly selected five fields of each well were photographed and counted using ImageJ software (NIH Image, Bethesda, USA). For invasion assays, the upper chamber of the Transwell plates were coated with 50 μL Matrigel (354234, BD, San Jose, USA, diluted 1:15) overnight at 37 ^oC. 5×10^4 cells

in 200 µL DMEM medium without FBS were added into the upper chamber of Matrigel-coated Transwell plates and 600 µL DMEM medium with 10% FBS was added into the lower chamber. After 24 h, cells in the upper chamber were removed and cells under the membrane of the Transwell plates were fixed, stained and counted. There were three duplicate wells for each group in one experiment and three independent experiments for each assay.

RNA-Seq and transcriptome analysis

Total RNA from adherent and suspension MDA-MB-231 cells were extracted using Trizol reagent (15596-026, Ambion, Austin, USA) and total RNA concentration and purity were detected by NanoDrop2000 (Thermo Fisher Scientific, Waltham, USA). RNA integrity was further verified by electrophoresis through a 1.5% (w/v) agarose gel. A Truseq RNA Sample Prep Kit (RS-122-2203, Illumina,San Diego, USA) was employed in cDNA library construction according to the manufacturer's instructions. Each library was sequenced using Illumina 2000 sequencer (Illumina, San Diego, USA). The raw data was filtered to remove the adapter sequences, low quality reads, higher N rate sequences and too short sequences. The remaining high-quality reads were mapped to the reference Ensembl human genome 19 using Tophat software. The expression quantity of each gene (fragments per kilobase of exon model per million mapped fragments, FPKM) was estimated using Cufflinks software. FDR (false discovery rate) < 0.05 and $|Log_2FC$ (fold change)$| \geq 2$ were used as the threshold for judging the significance of gene expression difference. The Illumina sequencing and foundation analysis were completed by Shanghai Majorbio Bio-pharm Biotechnology Co. (http://www.majorbio.com, Shanghai, China). Gene ontology (GO) and functional enrichment analysis were conducted on all identified differentially expressed genes (DEGs) using the Goatools software ($p \leq 0.05$). For pathway enrichment analysis, all DEGs were mapped to the terms in the KEGG database and searched for significantly enriched KEGG terms compared to the whole transcriptome background (q-value ≤ 0.05). The RNA-Seq data were deposited in NCBI's Sequence Read Archive (SRA) with accession number SRP119818.

Real-time quantitative PCR

Total RNA from cells were isolated using Trizol reagent (15596-026, Ambion, Austin, USA). 1 µg total RNA was reverse-transcribed into cDNA using the ReverAid™ First-Strand cDNA synthesis kit (K1622, Fermentas, Vilnius, Lithuania) following the manufacturer's protocol. Real-time PCR was conducted using SYBR Green PCR Reagents (RR820A, Takara, Dalian, China) and the CFX96™ Real-Time PCR Detection System (Bio-Rad, Hercules, USA). Fold changes of mRNA expressions were calculated using ΔΔCt analysis. Primers are shown in **Table S1**.

Western blot analysis

The suspension and adherent cells were lysed with RIPA buffer (P0013B, Beyotime, Shanghai, China) containing a protease inhibitor cocktail to harvest the total protein. Isolation of cytoplasmic/ nuclear proteins was programmed according to a previously established protocol. In brief, cells were lysed with 100 µL buffer (10 mM Hepes-NaOH, pH 7.9, 10 mM KCl, 1.5 mM $MgCl_2$, and 0.5 mM beta-mercaptoethanol) supplemented with protease inhibitor mixture and phosphatase inhibitors for 20 min on ice. 2 µL 10% NP-40 was added and centrifuged at 15,000 ×g for 15 min. The supernatant was cytoplasmic proteins. The pellet was washed with ice-cold PBS twice and lysed with 40 µL nuclei lysis buffer (10 mM Tris-HCl, pH 7.6, 420 mM NaCl, 0.5% NP-40, and 1 mM DTT, 2 mM $MgCl_2$ plus protease and phosphatase inhibitors) for 20 min on ice, then centrifuged. The extract was nuclear proteins and lower salt buffer (10 mM Tris-HCl, pH 7.6, 1 mM DTT, 2 mM $MgCl_2$ plus the protease and phosphatase inhibitors) was added to adjust the concentration of NaCl to 150 mM. Equal amounts of cell lysates were separated by 5-10% SDS-PAGE and electrophoretically transferred to a polyvinylidene difluoride (PVDF). After blocking for 1 h in tris buffered saline with tween (TBST) containing 5% non-fat milk at room temperature (RT), the membranes were incubated at 4 °C overnight with first antibodies: anti-COX-2 (1:1,000, Cell signaling technology, USA, 12282), anti-NFAT2 (1:1000, Abcam, Cambridge, USA, ab177464), anti-ICAM-1 (1:250, Santa Cruz, Dallas, USA, sc8439), anti-MUC1 (1:250, Santa Cruz, Dallas, USA, sc7313), anti-FN (1:1,000, Abcam, Cambridge, USA, ab6328), anti-Lamin B (1:250, Santa Cruz, Dallas, USA, sc6217) and anti-GAPDH (1:250, Santa Cruz, Dallas, USA, sc25778). The membranes were incubated with appropriate horseradish peroxidase-conjugated secondary antibodies (1:2,000, Beyotime, Shanghai, China) for 1 h at RT. Finally, the blots were detected with SuperSignal West Femto Maximum Sensitivity Substrate (34095, Thermo Scientific, Waltham, USA) and visualized by VersaDoc (Bio-Rad, Hercules,USA).

Intracellular calcium ion detection

Adherent cells were incubated with 2.5 µM Fluo-3AM (S1056, Beyotime, Shanghai, China) for 30

min at 37 °C. Then, the cells were washed and incubated other 30 min at 37 °C for esterase cleavage activation. For observation of calcium influx when cells detached, adherent cells loaded with Fluo-3AM were trypsinized and PBS containing calcium was added. Cells were shaken down gently into suspension. The adherent and suspension cells were observed by inverted fluorescence microscopy (Olympus IX71, Tokyo, Japan).

RNAi

siRNA oligonucleotides toward COX-2 and control siRNA were designed by BLOCK-iT™ RNAi Designer (Invitrogen, Carlsbad, USA) (**Table S2**) and synthesized by GenePharma. 100 pmol siRNA was transfected into BCCs with 5 μL Lipofectamine 2000 (11668-019, Invitrogen, Carlsbad, USA) for each well of 6-well plates. After 6 h, the transfected cells were harvested to suspension or adherent culture.

Preparation of polyacrylamide substrates

Different compliant polyacrylamide gels (PA gels) were prepared according to a previously established protocol [55]. In brief, 50 μL of 0.1 M NaOH was added to 12 mm circular coverslips and air dried. 50 μL 3-aminopropyltriethoxysilane (APES) (A3648, Sigma-Aldrich, Saint Louis, USA) was spread evenly onto the coverslip surface. After 5 min, the coverslips were rinsed with distilled H_2O to completely remove off the unreacted APES. Then, the coverslips were immersed with enough 0.5% glutaraldehyde in PBS for 30 min. The coverslips were washed with distilled H_2O and air dried. To polymerize, 20 μL polyacrylamide gel solutions with 0.1% w/v ammonium persulfate (A3678, Sigma-Aldrich, Saint Louis, USA) and 0.1% v/v tetramethyl-ethylenediamine (V900853, Sigma-Aldrich, Saint Louis, USA) was added onto chloro-silanated glass slides by dichlorodimethylsilane (40140, Sigma-Aldrich, Saint Louis, USA). The amino-silanated coverslips were placed on top of the polyacrylamide gel solutions. After 30 min, the polyacrylamide gels were soaked and washed with 50 mM HEPES buffer, then treated with 0.2 mg/mL sufosuccinimidyl-6-(4'-azido-2'-nitrophenylamino)-hexanoate (sulfo-SANPAH) (22589, Pierce Biotechnology, Rockford, USA) under a 365 nm ultra violet (UV) light for 10 min, two times. Then, the gels were coated with 50 μg/mL rat tail collagen-I protein overnight at 4 °C. The gels were washed with PBS three times before cell seeding.

F-actin staining

MDA-MB-231 cells were cultured on the PA gels with different stiffness (0.5 kPa, 5 kPa, 20 kPa) and TCPS plates for 2 d. For disruption of the cell cytoskeleton and inhibition of cell contraction, 0.5 μM cytochalasin D and 10 μM ROCK inhibitor Y27632 were used to treat cells for 1 h, respectively. Cells were incubated with rhodamine-labeled phalloidin (R415, Molecular Probess, Oregon, USA, diluted 1:30) at RT for 1 h, and the nuclei were stained with DAPI. Images were obtained using an inverted fluorescence microscope (Olympus IX71, Tokyo, Japan).

In vivo tumor models

Female Balb/c nu/nu mice, 6 weeks of age, were purchased from Animal Experimental Center of the Third Military Medical University. All animal experiments in this study were done at theAnimal Experimental Center of the Third Military Medical University and approved by Laboratory Animal Welfare and Ethics Committee of the Third Military Medical University. MDA-MB-231 cells that were adherent or suspensioncultured for 3 d (1×10^6 cells) were injected subcutaneously into the second left or right mammary gland of mice with Matrigel. The tumor volume was measured with a digital caliper once every 3 d (beginning 5 d after injection) using the formula $0.52 \times a \times b^2$, where in a and b are the largest and smallest diameters. After euthanizing the mice on day 21, the tumors were excised from the mice and weighed. For the experimental metastasis model, MDA-MB-231 cells adherent or suspension cultured for 3 d (5×10^5 cells) in 100 μL PBS were injected *via* tail vein. After 28 d, the lungs of the mice were harvested and weighed. The metastasis nodules on the lungs were counted under a dissection microscope.

To evaluate the effect of COX-2 on metastasis of suspension MDA-MB-231 cells, MDA-MB-231 cells were firstly infected with lentivirus vector (GenePharma, Shanghai, China) encoding green fluorescent protein (GFP). GFP-expressing MDA-MB-231 cells were transfected with COX-2-targeted siRNA (si-COX-2) or control siRNA (si-Ctrl) and cultured in adherent or suspension condition for 3 d, then subjected to tail vein injection. After 24 h, some mice were executed and lungs were fixed and sectioned for counting of GFP-positive cells (visible BCCs) and cleaved caspase 3-positive cells (apoptotic BCCs). Apoptosis rate was counted by the formula (cleaved caspase 3-positive cells) /(GFP-positive cells + cleaved caspase 3-positive cells). 28 days after injection, lungs of remaining mice were harvested and weighed.

Immunohistochemistry

Portions of tumors and lungs were fixed in 4% paraformaldehyde and embedded in paraffin. Five micrometer sections were used for immune-histological analysis using rabbit anti-cleaved caspase

3 (1:100, Abcam, ab32042, specifically reacts with human, not with mouse) and rabbit anti-COX-2 (1:200, Cell signaling technology, 12282). SP Kit (SP-9001, Zhongshan Golden Bridge Biotechnology, Beijing, China) and DAB Peroxidase Substrate Kit (ZLI-9017, Zhongshan Golden Bridge Biotechnology, Beijing, China) were used according to the manufacturers' protocols. For histology analysis, some sections were stained with hematoxylin-eosin (H-E) (C0105, Beyotime, Shanghai, China) according to the manufacturer's protocol. Three samples for each group were analyzed using an inverted light microscope (Olympus IX71).

Statistical analysis

Each experiment was repeated at least in triplicate and all data are presented as mean ± S.E. (standard error). The statistical analyses were conducted with GraphPad Prism software (version 6, GraphPad Software). Pairwise comparisons were made using a two-sample *t*-test (parametric data) or a Mann-Whitney test (nonparametric data).

Comparisons between multiple groups were made by one-way analysis of variance (ANOVA) followed by Tukey test (parametric data) or Kruskal-Wallis ANOVA (nonparametric data). $P< 0.05$ was considered statistically significant (*, $P< 0.05$; **, $P< 0.01$; #, $P< 0.001$).

Abbreviations

APES: aminopropyltriethoxysilane; BCCs: breast cancer cells; B-RAF: B-Raf proto-oncogene; CaN: calcineurin; COX-2: cyclooxygenase-2; CsA: cyclosporine A; CTCs: circulating tumor cells; CXB: celecoxib; CytoD: Cytochalasin D; DEGs: differentially expressed genes; ECM: extracellular matrix; EMT: epithelial-mesenchymal transition; ERK: extracellular regulated protein kinases; FBS: fetal bovine serum; FDR: false discovery rate; FN: fibronectin; FPKM: fragments per kilobase of exon model per million mapped fragments; GFP: green fluorescent protein; GO: gene ontology; H-E: hematoxylin-eosin; Her2: human epidermal growth factor receptor 2; ICAM-1: intercellular adhesion molecule 1; MUC1: mucin1; NFAT: nuclear factor of activated T cells; PA gels: polyacrylamide gels; PBS: phosphate buffer solution; PGE_2: prostaglandin E_2; PI: propidium iodide; Poly-HEMA: poly(2-hydroxyethyl methacrylate); PTGS2: prostaglandin-endoperoxide synthase 2; PVDF: polyvinylidene difluoride; RT: room temperature; SRA: sequence read archive; sulfo-SANPAH: sufosuccinimidyl-6-(4'-azido-2'-nitrophenylamino)-hexanoate; TAZ: WW domain-containing transcription regulator 1; TBST: tris buffered saline with tween; TCPS: tissue culture polystyrene; TGF-β1: transforming growth factor-β1; TrkB: neurotrophic receptor tyrosine kinase B; UV: ultra violet; YAP: Yes-associated protein.

Accession code

RNA-Seq data have been submitted to NCBI's Sequence Read Archive (SRA, http://www.ncbi.nlm.nih.gov/sra/) under the accession number SRP119818.

Acknowledgments

This research was supported by the National Natural Science Foundation of China Grant 11672051.

Supplementary Material

Supplementary figures and tables.
http://www.thno.org/v08p3722s1.pdf
Supplementary dataset S1.
http://www.thno.org/v08p3722s2.xls

Competing Interests

The authors have declared that no competing interest exists.

References

1. Engler AJ, Sen S, Sweeney HL, Discher DE. Matrix elasticity directs stem cell lineage specification. Cell. 2006; 126: 677-89.
2. Janson IA, Putnam AJ. Extracellular matrix elasticity and topography: material-based cues that affect cell function via conserved mechanisms. J Biomed Mater Res A. 2015; 103: 1246-58.
3. Chaudhuri O, Koshy ST, Branco da Cunha C, Shin JW, Verbeke CS, Allison KH, et al. Extracellular matrix stiffness and composition jointly regulate the induction of malignant phenotypes in mammary epithelium. Nat Mater. 2014; 13: 970-8.
4. Plodinec M, Loparic M, Monnier CA, Obermann EC, Zanetti-Dallenbach R, Oertle P, et al. The nanomechanical signature of breast cancer. Nat Nano. 2012; 7: 757-65.
5. Levental KR, Yu H, Kass L, Lakins JN, Egeblad M, Erler JT, et al. Matrix crosslinking forces tumor progression by enhancing integrin signaling. Cell. 2009; 139: 891-906.
6. Aragona M, Panciera T, Manfrin A, Giulitti S, Michielin F, Elvassore N, et al. A mechanical checkpoint controls multicellular growth through YAP/TAZ regulation by actin-processing factors. Cell. 2013; 154: 1047-59.
7. Ko P, Kim D, You E, Jung J, Oh S, Kim J, et al. Extracellular matrix rigidity-dependent sphingosine-1-phosphate secretion regulates metastatic cancer cell invasion and adhesion. Sci Rep. 2016; 6: 21564.
8. Ma JW, Zhang Y, Tang K, Zhang HF, Yin XN, Li Y, et al. Reversing drug resistance of soft tumor-repopulating cells by tumor cell-derived chemotherapeutic microparticles. Cell Res. 2016; 26: 713-27.
9. Polacheck WJ, Charest JL, Kamm RD. Interstitial flow influences direction of tumor cell migration through competing mechanisms. Proc Natl Acad Sci U S A. 2011; 108: 11115-20.
10. Wei SC, Fattet L, Tsai JH, Guo Y, Pai VH, Majeski HE, et al. Matrix stiffness drives epithelial-mesenchymal transition and tumour metastasis through a TWIST1-G3BP2 mechanotransduction pathway. Nat Cell Biol. 2015; 17: 678-88.
11. Chang SF, Chang CA, Lee DY, Lee PL, Yeh YM, Yeh CR, et al. Tumor cell cycle arrest induced by shear stress: Roles of integrins and Smad. Proc Natl Acad Sci U S A. 2008; 105: 3927-32.
12. Fernandez-Sanchez ME, Barbier S, Whitehead J, Bealle G, Michel A, Latorre-Ossa H, et al. Mechanical induction of the tumorigenic beta-catenin pathway by tumour growth pressure. Nature. 2015; 523: 92-5.
13. Wang N, Tytell JD, Ingber DE. Mechanotransduction at a distance: mechanically coupling the extracellular matrix with the nucleus. Nat Rev Mol Cell Biol. 2009; 10: 75-82.
14. Tajik A, Zhang Y, Wei F, Sun J, Jia Q, Zhou W, et al. Transcription upregulation via force-induced direct stretching of chromatin. Nat Mater. 2016; 15: 1287-96.
15. Buxboim A, Swift J, Irianto J, Spinler KR, Dingal PC, Athirasala A, et al. Matrix elasticity regulates lamin-A,C phosphorylation and turnover with feedback to actomyosin. Curr Biol. 2014; 24: 1909-17.

16. Martinac B. The ion channels to cytoskeleton connection as potential mechanism of mechanosensitivity. Biochim Biophys Acta. 2014; 1838: 682-91.
17. Formigli L, Meacci E, Sassoli C, Squecco R, Nosi D, Chellini F, et al. Cytoskeleton/stretch-activated ion channel interaction regulates myogenic differentiation of skeletal myoblasts. J Cell Physiol. 2007; 211: 296-306.
18. Yu M, Bardia A, Wittner BS, Stott SL, Smas ME, Ting DT, et al. Circulating breast tumor cells exhibit dynamic changes in epithelial and mesenchymal composition. Science. 2013; 339: 580-4.
19. Luo X, Mitra D, Sullivan RJ, Wittner BS, Kimura AM, Pan S, et al. Isolation and molecular characterization of circulating melanoma cells. Cell Rep. 2014; 7: 645-53.
20. Ting DT, Wittner BS, Ligorio M, Vincent Jordan N, Shah AM, Miyamoto DT, et al. Single-cell RNA sequencing identifies extracellular matrix gene expression by pancreatic circulating tumor cells. Cell Rep. 2014; 8: 1905-18.
21. Yu M, Ting DT, Stott SL, Wittner BS, Ozsolak F, Paul S, et al. RNA sequencing of pancreatic circulating tumour cells implicates WNT signalling in metastasis. Nature. 2012; 487: 510-3.
22. Labelle M, Begum S, Hynes RO. Direct signaling between platelets and cancer cells induces an epithelial-mesenchymal-like transition and promotes metastasis. Cancer Cell. 2011; 20: 576-90.
23. Malin D, Strekalova E, Petrovic V, Rajanala H, Sharma B, Ugolkov A, et al. ERK-regulated alphaB-crystallin induction by matrix detachment inhibits anoikis and promotes lung metastasis *in vivo*. Oncogene. 2015; 34: 5626-34.
24. Celil Aydemir AB, Minematsu H, Gardner TR, Kim KO, Ahn JM, Lee FY. Nuclear factor of activated T cells mediates fluid shear stress- and tensile strain-induced COX-2 in human and murine bone cells. Bone. 2010; 46: 167-75.
25. Fermor B, Weinberg JB, Pisetsky DS, Misukonis MA, Fink C, Guilak F. Induction of cyclooxygenase-2 by mechanical stress through a nitric oxide-regulated pathway. Osteoarthritis Cartilage. 2002; 10: 792-8.
26. Liu F, Mih JD, Shea BS, Kho AT, Sharif AS, Tager AM, et al. Feedback amplification of fibrosis through matrix stiffening and COX-2 suppression. J Cell Biol. 2010; 190: 693-706.
27. Zhang XM, LV YH. Suspension state increases reattachment of breast cancer cells by up-regulating lamin A/C. Biochim Biophys Acta. 2017; 1864: 2272-82.
28. Whipple RA, Cheung AM, Martin SS. Detyrosinated microtubule protrusions in suspended mammary epithelial cells promote reattachment. Exp Cell Res. 2007; 313: 1326-36.
29. Hou J, Zhou Z, Chen X, Zhao R, Yang Z, Wei N, et al. HER2 reduces breast cancer radiosensitivity by activating focal adhesion kinase in vitro and *in vivo*. Oncotarget. 2016; 7: 45186-98.
30. Bartosh TJ, Ullah M, Zeitouni S, Beaver J, Prockop DJ. Cancer cells enter dormancy after cannibalizing mesenchymal stem/stromal cells (MSCs). Proc Natl Acad Sci USA. 2016; 113: E6447-E56.
31. Zheng H, Li Y, Wang Y, Zhao H, Zhang J, Chai H, et al. Downregulation of COX-2 and CYP 4A signaling by isoliquiritigenin inhibits human breast cancer metastasis through preventing anoikis resistance, migration and invasion. Toxicol Appl Pharmacol. 2014; 280: 10-20.
32. Beauséjour M, Noël D, Thibodeau S, Bouchard V, Harnois C, Beaulieu JF, et al. Integrin/Fak/Src-mediated regulation of cell survival and anoikis in human intestinal epithelial crypt cells: selective engagement and roles of PI3-K isoform complexes. Apoptosis. 2012; 17: 566-78.
33. Mern DS, Hoppe-Seyler K, Hoppe-Seyler F, Hasskarl J, Burwinkel B. Targeting Id1 and Id3 by a specific peptide aptamer induces E-box promoter activity, cell cycle arrest, and apoptosis in breast cancer cells. Breast Cancer Res Treat. 2010; 124: 623-33.
34. Zhang H, Kim JK, Edwards CA, Xu Z, Taichman R, Wang CY. Clusterin inhibits apoptosis by interacting with activated Bax. Nat Cell Biol. 2005; 7: 909-15.
35. Shen CJ, Chan SH, Lee CT, Huang WC, Tsai JP, Chen BK. Oleic acid-induced ANGPTL4 enhances head and neck squamous cell carcinoma anoikis resistance and metastasis via up-regulation of fibronectin. Cancer Lett. 2017; 386: 110-22.
36. Douma S, Van Laar T, Zevenhoven J, Meuwissen R, Van Garderen E, Peeper DS. Suppression of anoikis and induction of metastasis by the neurotrophic receptor TrkB. Nature. 2004; 430: 1034-9.
37. Boisvert-Adamo K, Aplin AE. B-RAF and PI-3 kinase signaling protect melanoma cells from anoikis. Oncogene. 2006; 25: 4848-56.
38. Aceto N, Bardia A, Miyamoto DT, Donaldson MC, Wittner BS, Spencer JA, et al. Circulating tumor cell clusters are oligoclonal precursors of breast cancer metastasis. Cell. 2014; 158: 1110-22.
39. Ristimaki A, Sivula A, Lundin J, Lundin M, Salminen T, Haglund C, et al. Prognostic significance of elevated cyclooxygenase-2 expression in breast cancer. Cancer Res. 2002; 62: 632-5.
40. Sano H, Kawahito Y, Wilder RL, Hashiramoto A, Mukai S, Asai K, et al. Expression of cyclooxygenase-1 and -2 in human colorectal cancer. Cancer Res. 1995; 55: 3785-9.
41. Hida T, Yatabe Y, Achiwa H, Muramatsu H, Kozaki K, Nakamura S, et al. Increased expression of cyclooxygenase-2 occurs frequently in human lung cancers, specifically in adenocarcinomas. Cancer Res. 1998; 58: 3761-4.
42. Denkert C, Kobel M, Berger S, Siegert A, Leclere A, Trefzer U, et al. Expression of cyclooxygenase-2 in human malignant melanoma. Cancer Res. 2001; 61: 303-8.
43. Tucker ON, Dannenberg AJ, Yang EK, Zhang F, Teng L, Daly JM, et al. Cyclooxygenase-2 expression is up-regulated in human pancreatic cancer. Cancer Res. 1999; 59: 987-90.
44. Greenhough A, Smartt HJ, Moore AE, Roberts HR, Williams AC, Paraskeva C, et al. The COX-2/PGE2 pathway: key roles in the hallmarks of cancer and adaptation to the tumour microenvironment. Carcinogenesis. 2009; 30: 377-86.
45. Gupta RA, Dubois RN. Colorectal cancer prevention and treatment by inhibition of cyclooxygenase-2. Nat Rev Cancer. 2001; 1: 11-21.
46. Zelenay S, van der Veen AG, Bottcher JP, Snelgrove KJ, Rogers N, Acton SE, et al. Cyclooxygenase-dependent tumor growth through evasion of immunity. Cell. 2015; 162: 1257-70.
47. Rao A, Luo C, Hogan PG. Transcription factors of the NFAT family: regulation and function. Annu Rev Immunol. 1997; 15: 707-47.
48. Lopez-Rodriguez C, Aramburu J, Rakeman AS, Copeland NG, Gilbert DJ, Thomas S, et al. NF-AT5: the NF-AT family of transcription factors expands in a new direction. Cold Spring Harb Symp Quant Biol. 1999; 64: 517-26.
49. Quang CT, Leboucher S, Passaro D, Fuhrmann L, Nourieh M, Vincent-Salomon A, et al. The calcineurin/NFAT pathway is activated in diagnostic breast cancer cases and is essential to survival and metastasis of mammary cancer cells. Cell Death Dis. 2015; 6: e1658.
50. Yiu GK, Toker A. NFAT induces breast cancer cell invasion by promoting the induction of cyclooxygenase-2. J Biol Chem. 2006; 281: 12210-7.
51. Cho S, Irianto J, Discher DE. Mechanosensing by the nucleus: from pathways to scaling relationships. J Cell Biol. 2017; 216: 305-15.
52. Ingber DE. Cellular tensegrity: defining new rules of biological design that govern the cytoskeleton. J Cell Sci. 1993; 104 613-27.
53. Ingber DE, Wang N, Stamenovic D. Tensegrity, cellular biophysics, and the mechanics of living systems. Rep Prog Phys. 2014; 77: 046603.
54. Zhang Y, Lu H, Dazin P, Kapila Y. Squamous cell carcinoma cell aggregates escape suspension-induced, p53-mediated anoikis: fibronectin and integrin alphav mediate survival signals through focal adhesion kinase. J Biol Chem. 2004; 279: 48342-9.
55. Tse JR, Engler AJ. Preparation of hydrogel substrates with tunable mechanical properties. Curr Protoc Cell Biol. 2010; Chapter 10: Unit 10 16.